Polymer Chemistry

ROYAL SOCIETY OF CHEMISTRY

PAPER

View Article Online
View Journal | View Issue

Cite this: *Polym. Chem.*, 2021, **12**, 105

Functional nanostructures by NiCCo-PISA of helical poly(aryl isocyanide) copolymers†

Sètuhn Jimaja, [a,b,c] Yujie Xie, [a,b] Jeffrey C. Foster, [b] Daniel Taton, [c] Andrew P. Dove *[b] and Rachel K. O'Reilly *[b]

Herein, we present a straightforward and versatile methodology to achieve functional polymeric nano-objects that contain helical cores. Nickel-catalysed coordination polymerisation-induced self-assembly (NiCCo-PISA) of helical poly(aryl isocyanide) amphiphilic diblock copolymers was conducted, affording micelles containing controllable quantities of activated ester groups (*i.e.* pentafluorophenyl esters) in the core that were subsequently modified using post-polymerisation modification (PPM) with amine nucleophiles. Three amines bearing different functionalities (alcohol, trifluoro and a maleimide dye) were successfully introduced into the nano-object cores as verified *via* NMR and FT-IR spectroscopy, while the retention of helicity within the resulting diblock copolymers was confirmed by circular dichroism (CD) spectroscopy. Changes in nanostructure morphology following modification were monitored by dynamic light-scattering (DLS), confirming the disassembly of the nano-objects when the core hydrophilicity was increased through the introduction of polar functionalities. These readily-synthesised and modified nanostructures containing helical cores are valuable scaffolds for use in applications such as circularly polarised luminescence, enantioselective chemistry or chiral separation.

Received 1st June 2020,
Accepted 22nd July 2020

DOI: 10.1039/d0py00791a

rsc.li/polymers

Introduction

Post-polymerisation modification (PPM) is a versatile approach that has been widely employed to introduce functionality to polymeric materials.[1–4] The PPM approach bypasses the potentially time-consuming steps of synthesising novel functional monomers and precludes difficulties arising from the protection and deprotection of functionalities incompatible with polymerisation processes. Thus, PPM often reduces the number of synthetic steps required for material syntheses and provides precursor materials that can be modified with a wide variety of functional groups.[5–15]

For nanomaterials, reactive functionality provides a convenient and polyvalent means of introducing valuable moieties such as dyes,[16–18] catalysts or drugs.[19] PPM can also be employed to dynamically modify nanostructure properties, endowing such constructs with the capability to respond to environmental stimuli.[20–23] For example, Rifaie-Graham *et al.* developed a diblock copolymer system that was modified through two PPM steps to incorporate donor–acceptor Stenhouse adduct-derived dyes with distinct excitation wavelengths. The polymersomes assembled from these copolymers exhibited light-responsive permeability-switch behaviour. The polymersomes were loaded with complementary enzymes, one type of polymersome with glucose oxidase and the other with horseradish peroxidase. Treatment of the resulting suspension with purpurogallin led to the formation of a wavelength-selective biocatalysis cascade that oxidised glucose on demand, which could be followed spectrophotometrically by measuring the chemiluminescent oxidation of purpurogallin.[24] Wooley and co-workers developed polyphosphoester block copolymers fitted with alkyne[25] or alkene[26,27] pendant groups that could be readily functionalised using thiol nucleophiles. They demonstrated that PPM of these alkyne-containing phosphodiester scaffolds *via* thiol–yne chemistry allowed for facile modification of the polymer charge in water. Self-assembly of the modified copolymers yielded micelles with differential surface charge—non-ionic, anionic, cationic and zwitterionic—impacting the cytotoxicity of the particles toward mouse macrophage cells. In this instance, PPM enabled the creation of a library of polymers from a single scaffold.

Pentafluorophenol (PFP) esters are activated electrophiles reactive towards amines and alcohols that can be employed in PPM. For the synthesis of such scaffolds by controlled radical polymerisation, both pentafluorophenyl methacrylate (PFPMA)

[a]*Department of Chemistry, University of Warwick, Coventry CV4 7AL, UK*
[b]*School of Chemistry, University of Birmingham, Edgbaston B15 2TT, UK. E-mail: r.oreilly@bham.ac.uk, a.dove@bham.ac.uk*
[c]*Laboratoire de Chimie des Polymères Organiques, Université de Bordeaux/CNRS École Nationale Supérieure de Chimie, de Biologie & de Physique, 33607 Cedex Pessac, France*

†Electronic supplementary information (ESI) available. See DOI: 10.1039/d0py00791a

and pentafluorophenyl acrylate (PFPA) have been exploited as comonomers to incorporate the reactive functionality.[28–32] In one example, Meijer and co-workers developed single-chain polymeric nanoparticles (SCNPs) composed of polyacrylate copolymers containing PFPA.[33] This system was readily modified by reaction with different amines to affix the SCNPs with precise functionality; in this case, ligands capable of binding copper for the catalysis of azide–alkyne cycloaddition and depropargylation reactions, or Jeffamine for photosensitisation.[33] More recently, PFPMA was employed by Couturaud *et al.* as a core-forming monomer for reversible addition–fragmentation chain transfer (RAFT)-mediated polymerisation-induced self-assembly (PISA) in DMSO.[34] The resulting nanostructures were subsequently cross-linked *via* the activated ester groups with disulphide-containing diamine crosslinkers to achieve redox-responsive nanoparticles that degraded in the presence of reducing agents.

PFP-derived monomers can undergo PISA in DMSO due to their high solubility and tendency to produce polymers that become insoluble upon elongation. Based on our successful implementation of nickel-catalysed coordination-PISA (NiCCo-PISA) of aryl isocyanides in DMSO,[35] we hypothesised that a PFP aryl isocyanide could be used as a core-forming monomer either as such or *via* copolymerisation with menthyl-ester aryl isocyanide (**MAIC**), while a PEG-ester aryl isocyanide (**PAIC**) served as the stabilising block.[36] Wu and co-workers developed such a PFP aryl isocyanide (**FAIC**) comonomer to introduce electrophile handles into helical polyisocyanides (PIC).[37–39] They demonstrated that **FAIC** readily polymerised under the same conditions as **MAIC**. Based on the similar solvophobicity of **FAIC** and **MAIC**, their copolymerisation represented an ideal system for the synthesis of helical and functionalisable nanostructures using NiCCo-PISA. Further, we reasoned that the resulting nanostructures would maintain their helicity subsequent to modification with various functional nucleophiles due to the static nature of the PIC helices.

In this study, we explore the synthesis, helicity, and self-assembly behaviour of P(**PAIC**)-*b*-P(**MAIC**-*co*-**FAIC**) block copolymer nanostructures synthesised by NiCCo-PISA. Further, we investigate the possibility of their modification with different nucleophiles and the influence of added functionality on the nano-objects' size, stability and helicity retention. The combination of the simplicity of synthesising helix-containing nanostructures by NiCCo-PISA and the wide range of potential modifications possible by PPM provides a modular platform for the preparation of functional and helical nanomaterials.

Results and discussion

Functionalisable NiCCo-PISA micelles

To develop functionalised particles *via* NiCCo-PISA, it was necessary to introduce **FAIC** to the formulation without disrupting the polymerisation or self-assembly processes. In order to investigate the former, **MAIC** and **FAIC** were copolymerised in THF, a common solvent for both homopolymers,

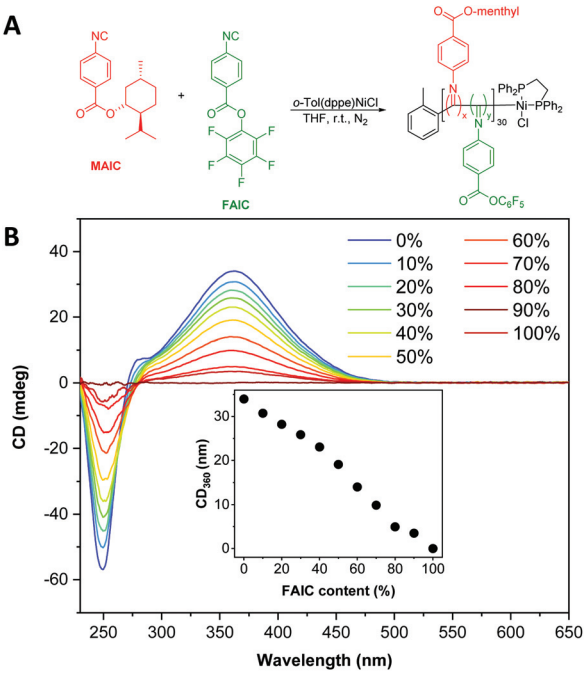

Fig. 1 (A) Synthesis scheme of P(**MAIC**)$_x$-*co*-P(**FAIC**)$_y$ where $x + y = 30$. (B) CD spectra (THF, 0.5 mg mL^{-1}) of P(**MAIC**)$_x$-*co*-P(**FAIC**)$_y$ copolymers with **FAIC** content ranging from 0 to 100 mol%.

aiming for a degree of polymerisation (DP) of 30 and using different comonomer feed ratios to achieve P(**MAIC**-*co*-**FAIC**) copolymers containing 0–100 mol% of **FAIC** units (Fig. 1A). After purification by repeated precipitation in methanol, analysis of the copolymers by SEC indicated no apparent differences in molecular weight distribution between the copolymers, with number average molecular weights (M_n) ranging between 4.4–4.5 kDa and dispersity (D_M) between 1.13–1.21 (Fig. S5†) across the series.

The successful incorporation of **FAIC** units into the copolymers was evidenced by ^{19}F NMR spectroscopy (Fig. S6†). In particular, the broad signals at −153, −158 and −162 ppm in the ^{19}F NMR spectra corresponded to the incorporated PFP moieties, proved in agreement with the monomer spectrum. The fluorine signal intensity increased with the quantity of **FAIC** present in the copolymer with the exception of the P(**FAIC**)$_{30}$ homopolymer, likely as a consequence of its poor solubility in chloroform decreasing its signal intensity. Overall, these data demonstrated that copolymerisation of **FAIC** with **MAIC** did not appear to negatively influence molecular weight or molecular weight distribution (MWD).

The copolymers exhibited a clear signal at λ = 360 nm, assigned to the n–π^* transition of the PIC backbone C=N, consistent with previous literature reports.[46–48] The helicity of the copolymers, as quantified by the strength of the signal at λ = 360 nm in the CD spectra, was found to vary linearly with the content of **MAIC** (*i.e.* the chiral monomer), decreasing until no CD absorption was present for P(**FAIC**)$_{30}$ in the absence of chiral information (Fig. 1B).

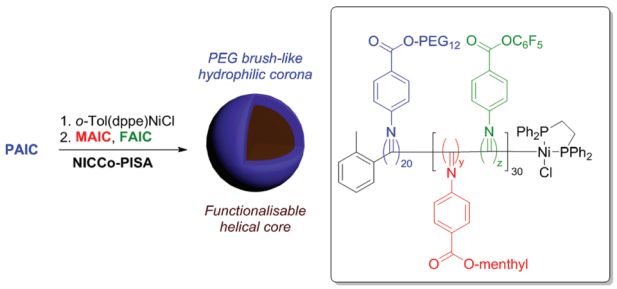

Scheme 1 NiCCo-PISA to prepare functional P(**PAIC**)$_{20}$-*b*-(P(**MAIC**)$_x$-*co*-P(**FAIC**)$_y$)$_{30}$ diblock copolymer nano-objects.

We next sought to understand the impact of including the relatively more hydrophobic **FAIC** comonomer in our PISA formulation. To this end, NiCCo-PISA was conducted using **PAIC** to form the stabiliser block with $DP_{P(PAIC)}$ = 20 and $DP_{solvophobic}$ (*i.e.* $DP_{P(MAIC)}$ + $DP_{P(FAIC)}$) of 30 aiming for spherical micelles (Scheme 1). Different **FAIC** loadings were targeted in a series of experiments: 20, 50 and 100 mol% of the core block. The resulting P(**PAIC**)$_{20}$-*b*-(P(**MAIC**)$_y$-*co*-P(**FAIC**)$_z$)$_{30}$ diblock copolymers were named based on their **FAIC** content: **D20%**, **D50%** and **D100%**. A control containing no PFP moieties (**D0%**) was prepared to verify the stability of **MAIC** and **PAIC** units toward nucleophiles. SEC of the purified **D0%**, **D20%** and **D50%** diblock copolymers displayed no detectable differences in MWD, indicating that the polymerisation process was not impacted by the incorporation of **FAIC** as demonstrated earlier for the P(**MAIC**)$_x$-*co*-P(**FAIC**)$_y$ series. In contrast, the **D100%** copolymer showed at least two distinct populations, hinting that the self-assembly had an impact on the growth of the polymer as seen in our previous study on NiCCo-PISA.

DLS analysis of the diblock copolymer assemblies obtained from NiCCo-PISA was conducted to ensure that the particle size distribution was not affected by the incorporation of **FAIC** into the copolymer. Indeed, no major change in size was detected for **D20%** or **D50%** compared to **D0%** (Fig. 2). However, for **D100%**, the size distribution and correlogram indicated that some aggregation was occurring, likely caused by their increased core hydrophobicity.

The diblock copolymers were also analysed by CD spectroscopy (Fig. 3), showing that helicity was retained during the self-assembly process, as was presented previously for NiCCo-PISA to achieve P(**PAIC**)$_{20}$-*b*-P(**MAIC**)$_{30}$. However, a decrease in the CD signal was observed with increasing **FAIC** content, concordant with the CD analysis conducted on the P(**MAIC**)$_x$-*co*-P(**FAIC**)$_y$ series, resulting from the reduced proportion of chiral **MAIC** units in the core-forming blocks.

Functionalisation with ethanolamine and trifluoroethylamine

PPM of **D0%**, **D20%** and **D50%** using different primary amine nucleophiles was then evaluated (Scheme 2). Nucleophiles were chosen with groups that could be easily detected following PPM. In particular, we supposed that successful incorporation of ethanolamine (EOA) would decorate the copolymer

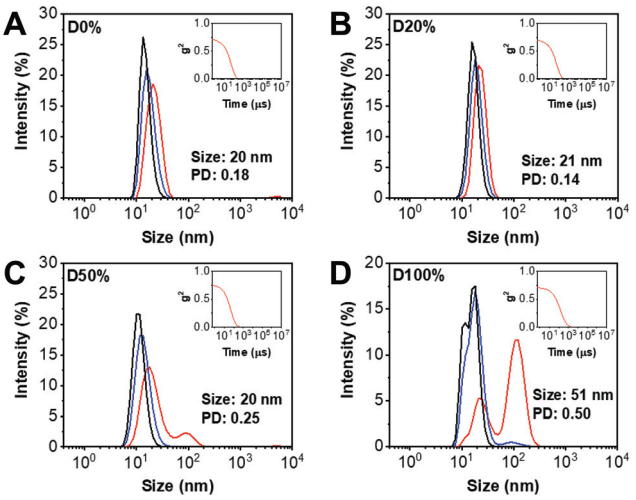

Fig. 2 Size distributions of (A) **D0%**, (B) **D20%**, (C) **D50%** and (D) **D100%** in DMSO obtained by DLS (1 mg mL^{-1}). The intensity (red line), volume (blue line) and number (black line) distributions are displayed. The insets show the correlograms.

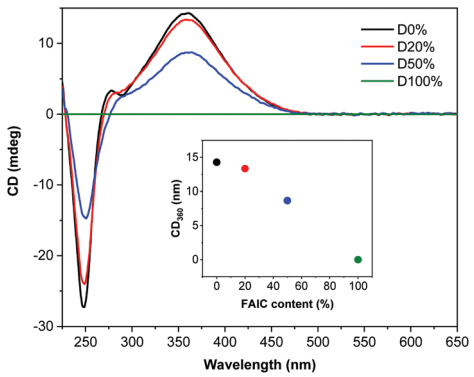

Fig. 3 CD (THF, 0.5 mg mL^{-1}) spectra of P(**PAIC**)$_{20}$-*b*-(P(**MAIC**)$_y$-*co*-P(**FAIC**)$_z$)$_{30}$ with 0, 20, 50 and 100 mol% of **FAIC**.

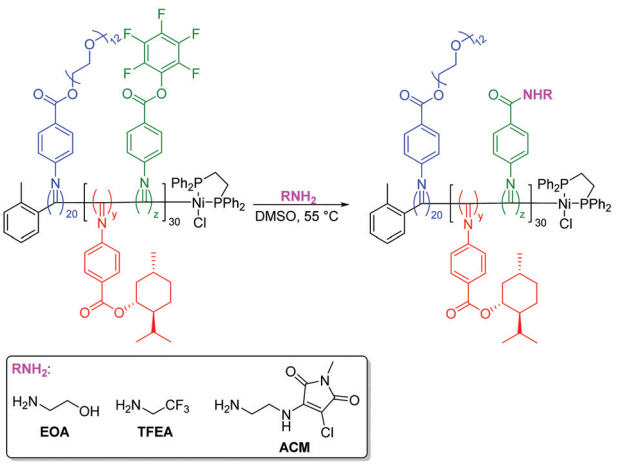

Scheme 2 PPM of P(**PAIC**)$_{20}$-*b*-(P(**MAIC**)$_y$-*co*-P(**FAIC**)$_z$)$_{30}$ with various primary amines: EOA, TFEA, and amine chloride maleimide dye.

with alcohol functionalities that should be detectable by FT-IR while trifluoroethylamine (TFEA) would introduce a new fluorine handle that could be followed using ^{19}F NMR spectroscopy. In addition, substitution with EOA was expected to drastically alter the polarity of the nanoparticle cores.

D0%, **D20%** and **D50%** were treated *in situ* with EOA and TFEA directly following NiCCo-PISA. These aminolysis reactions were carried out in the absence of base to avoid hydrolysis of the PFP esters.[34] An excess of amine was thus employed to ensure quantitative conversion to amide product. The reactions were allowed to stir for 24 h before an aliquot was taken and purified by dialysis to remove unreacted amine and phenolic by-products prior to analysis.

SEC analysis of the copolymers before and after substitution showed no significant change in MWD for **D20% + EOA**, **D20% + TFEA**, or **D50% + TFEA**, while high molecular weight tailing was observed for **D50% + EOA** (Fig. 4 and Fig. S7†). In the case of **D50% + EOA**, the broad MWD was attributed to interaction of the installed alcohol and amide functionalities with the SEC columns while in the case of **D50% + TFEA**, only the amides interacted with the column.

By FT-IR, several bands revealed the success and completion of the substitution reactions. First, a broad band at 3350 cm^{-1} indicated the presence of O–H (alcohol) and N–H (amide) groups and therefore the successful insertion of EOA into the copolymer (Fig. 5). The signal's strength was directly related to the quantity of the associated functionality; thus a stronger signal was evident for **D50% + EOA** compared to **D20% + EOA**. The absence of amide and alcohol signals for **D0% + EOA** demonstrated the stability of **MAIC** and **PAIC** to the reaction conditions. In addition, the absence of four bands in particular indicated the successful substitution of PFP units: 1761 cm^{-1} (C═O) and 1246 cm^{-1} (C–O) associated with the ester group; 1516 cm^{-1} (C═C) for the PFP aromatic unit and 1037 cm^{-1} for C–F (Fig. S8†). Their disappearance suggested the aminolysis reaction reached completion. A similar FT-IR spectroscopic analysis was performed for **D0%**, **D20%** and **D50%** after treatment with TFEA (Fig. S9†). It is noteworthy that the unreacted copolymers were purified by dialysis and the absence of COOH signal confirms the stability of the PFP units in aqueous environment.

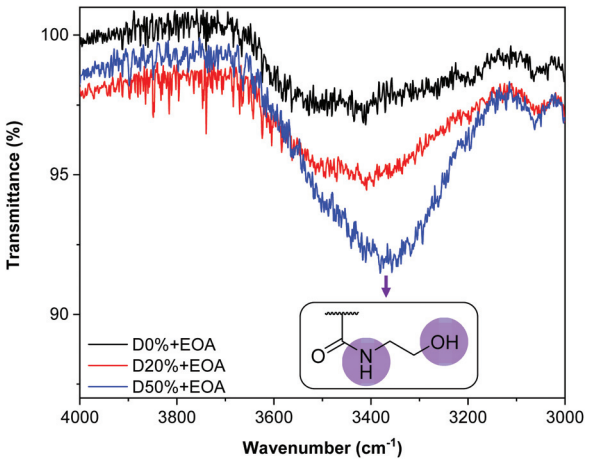

Fig. 5 FT-IR of **D0%** (black), **D20%** (red) and **D50%** (blue) following substitution reaction with **EOA**.

To further verify the consumption of PFP units, ^{19}F NMR spectroscopy of **D0%**, **D20%** and **D50%** before and after reaction with EOA or TFEA was conducted (Fig. 6 and Fig. S10†). The complete disappearance of these signals in the presence of amine suggested quantitative conversion during aminolysis. The absence of signals associated with molecular PFP also showed that the reaction by-product, pentafluorophenol, was successfully removed during the purification step. In the case of the TFEA substituted copolymers, *i.e.* **D20% + TFEA** and **D50% + TFEA**, the appearance of a new singlet at −72 ppm, assigned to the installed CF_3 group (Fig. 6), indicated the successful incorporation of TFEA. The broadened signal relative to the spectrum of the pure monomer provided further evidence of the attachment of CF_3 to the rigid copolymer chain. All copolymers were also analysed by ^{1}H NMR spectroscopy, where a new signal could be detected for **D50% + EOA** in concordance with the EOA CH_2 protons at 2.65 ppm (Fig. S11 and S12†).

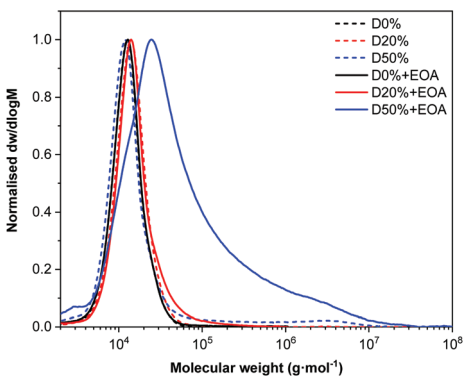

Fig. 4 Normalised SEC RI molecular weight distributions (THF + 2% v/v NEt_3, 40 °C, PS standards) of **D0%**, **D20%**, and, **D50%** and before and after treatment with EOA and purification by dialysis.

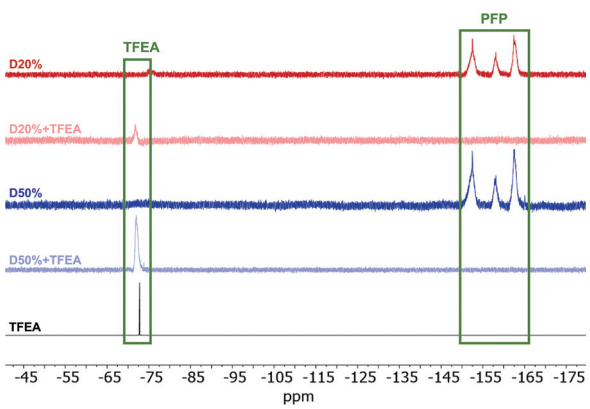

Fig. 6 ^{19}F NMR spectra of **D20%** and **D50%** in $CDCl_3$ (377 MHz, 298 K) before and after treatment with TFEA and purification by dialysis. The ^{19}F NMR spectrum of TFEA is also provided for comparison.

Table 1 Characterisation of **D0%**, **D20%** and **D50%** before and after treatment with EOA or TFEA

Polymer	D_h [a] (nm)	$M_{n,\,SEC}$ [b] (kDa)	$Đ_M$ [b]	CD_{360} [c] (mdeg)
D0%	20 (0.18)	11.2	1.24	14
D0% + EAO	20 (0.16)	11.4	1.22	—
D0% + TFEA	20 (0.17)	11.4	1.25	—
D20%	21 (0.14)	12.4	1.24	13
D20% + EOA	19 (0.17)	13.5	1.38	13
D20% + TFEA	18 (0.21)	13.0	1.20	13
D50%	20 (0.25)	10.5	1.34	9
D50% + EOA	34 (1.00)	—[d]	—[d]	8
D50% + TFEA	23 (0.32)	—[d]	—[d]	8

[a] Particle size measured by DLS with PD in parenthesis. [b] Determined by SEC (THF + 2% v/v NEt_3) using PS standards. [c] CD (THF, 0.5 mg mL^{-1}) signal at λ = 360 nm. [d] Molecular weight distribution was outside the calibration range.

The nano-object suspensions obtained from NiCCo-PISA and following PPM were also analysed by DLS (Fig. S13, Fig. S14† and Table 1) to verify their stability towards changes in core polarity from substitution of the PFP units. In brief, the size of the assemblies did not change for **D0% + EOA** and **D0% + TFEA**, indicating a good stability of the non-reactive nanostructure to the reaction conditions. Similarly, no change was found in the hydrodynamic diameters (D_h) of the **D20 + EAO**, **D20% + TFEA** and **D50% + TFEA** nanostructures. However, there was a clear indication of a size change for **D50% + EOA**, where the D_h after substitution increased from 20 to 34 nm and the size distribution (PD) from 0.25 to 1. This broad distribution of sizes can be explained by the increase in polarity and therefore solubility of the nanostructure's core, with their overall increase in solvophilicity leading to a partial disassembly of the nano-objects.

CD spectroscopy was employed to determine the change in helicity after aminolysis (Fig. 7). No significant changes were observed for any of the four copolymers when comparing spectra before and after PPM. The signal at λ = 360 nm remained constant at *ca.* 13 mdeg and 9 mdeg for the **D20%** and **D50%** substituted copolymers, respectively, while the signal at 250 nm decreased slightly. This latter absorption band was derived from the PFP aromatic rings in the copolymer scaffold and therefore was expected to decrease subsequent to substitution. These data confirmed the stability of the helical backbone to the reaction conditions and their resilience to the substitution of 20% or 50% of the core units.

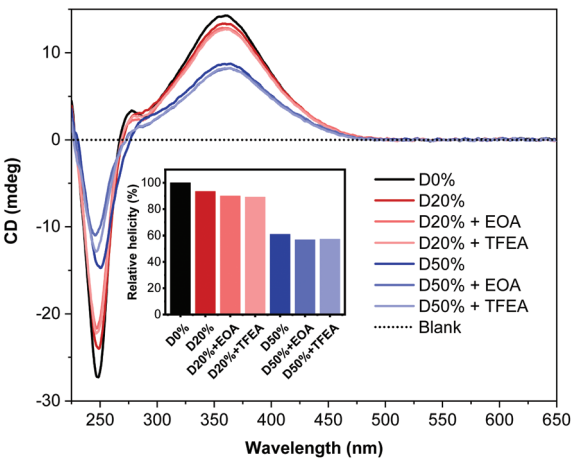

Fig. 7 CD (THF, 0.5 mg mL^{-1}) spectra of **D0%**, **D20%**, and, **D50%** before and after treatment with EOA or TFEA and purification by dialysis. The inset shows the helicity (CD at λ = 360 nm) of the copolymers compared to **D0%**.

Functionalisation with maleimide dye

To further leverage PPM to study changes in the self-assembly behaviour and composition of the diblock copolymer nanostructures, a fluorescent aminochloromaleimide (ACM) dye was synthesised (Scheme 2, see also ESI†) for introduction into the nano-object cores. Substituted maleimides like ACM possess solvent-dependent fluorescence lifetimes and emissions, which have been used extensively in our group for chemico-fluorescent responsive copolymers, fluorescent nanogels and the labelling of proteins, enzymes and polymers.[18,40–44] Following PPM, the copolymers were analysed as before.

By FT-IR, decreases in the **FAIC** signals were detectable for both reactions along with an increase of the amide (N–H) signal (Fig. S15†), signifying some, but incomplete, ACM incorporation. Observation of the signal at 1760 cm^{-1} assigned to the amide function (C═O) indicated there were still PFP units in both **D20% + ACM** and **D50% + ACM** (Fig. 8A). However, these signals were substantially broader following substitution. We reasoned that the resonance associated with the newly formed amides could also occupy this region, complicating calculation of conversion. Thus, the following spectroscopic analyses are more qualitative than quantitative and were simply used to confirm the presence or absence of dye and to evaluate the dye's environment. Interestingly, PFP units were still detected after the incomplete reactions which demonstrated their stability under the reaction conditions.

SEC analysis of the dye-substituted copolymer showed MWDs for **D0% + ACM** and **D20% + ACM** similar to their parent copolymers, while the **D50% + ACM** copolymer exhibited clear tailing in this region (Fig. S16†). Here, the ACM-derived secondary amine and/or imide functionalities were assumed to interact with the SEC column in a similar manner to the alcohol functionalities of the **D50% + EOA** copolymer.

CD spectroscopy showed an increase of the CD signals at λ = 250 nm and 360 nm for both dye-substituted copolymers (Fig. 8B). It was known that the ACM unit is UV-active in these regions as evidenced by its UV/Vis spectrum. It should also be noted that the ACM moiety possesses no inherent chirality. CD spectroscopy measures the absorbance of chiral species; thus, the increase in absorbance at *ca.* λ = 360 nm in the CD spectra of **D20% + ACM** and **D50% + ACM** further corroborated the successful introduction of ACM into the helical environment of the diblock copolymer.

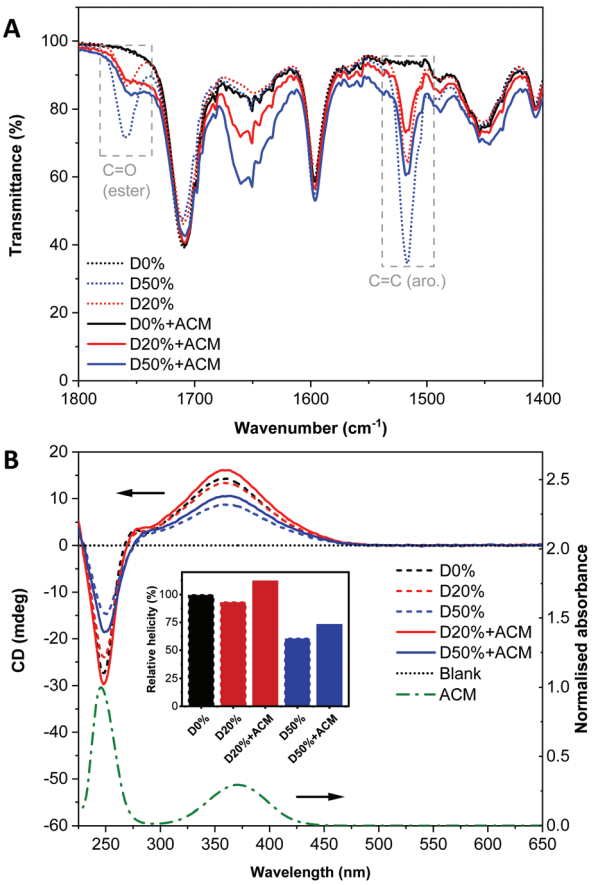

Fig. 8 (A) FT-IR and (B) CD (THF, 0.5 mg mL^{-1}) spectra of the **D0%** (black), **D20%** (red) and **D50%** (blue) copolymers before (dotted lines) and after PPM with ACM (solid lines). UV/Vis spectrum (THF, 0.5 mg mL^{-1}) of free ACM. The inset shows the helicity (CD at λ = 360 nm) of the copolymers compared to **D0%**.

As before, the obtained diblock copolymer nanostructures were analysed by DLS. The **D20% + ACM** copolymer formed micelles of similar size to the unmodified diblock copolymer (22 *vs.* 21 nm). The size distributions and correlogram for **D50% + ACM** indicated a possible partial disassembly of the nanostructures with a D_h of 16 nm and a PD of 0.37 *vs.* 0.25 for the unmodified copolymer (Fig. S17†). The higher hydrophilicity of the dye compared with the PFP units likely increased the solvability of the core, inducing increased solvation of the micelle unimer constituents.

Fluorescence spectrophotometry was utilised to monitor ACM fluorescence from the modified diblock copolymers. The original polymer, **D0%**, was not fluorescent in the absence of dye substitution. In contrast, an emission band was detected at λ_{em} = 488 nm for both of the dye-substituted polymers when excited at λ_{ex} = 375 nm in THF, in line with the fluorescence emission of the free ACM. Moreover, a solution containing a mixture of the copolymer **D0%** and the free dye displayed a signal at the same wavelength, proving that the copolymer itself did not influence λ_{em} (Fig. S18†). After transfer of the species to water, λ_{em} for nanostructures of **D20% + ACM** and **D50% + ACM** shifted to 510 nm (Δ_λ = 22 nm). By comparison,

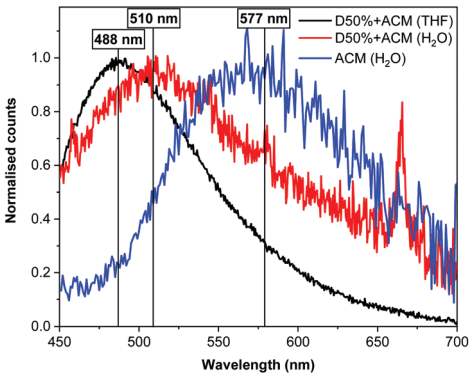

Fig. 9 Fluorescence spectra (λ_{ex} = 375 nm) for **D50% + ACM** and free ACM in THF or H_2O.

the redshift in emission of the free dye was more substantial (λ_{em} = 577 nm, Δ_λ = 89 nm). The observed differences in emission in H_2O between the polymer-bound and free dye are consistent with previous studies from our group and reflect the environmental dependence of ACM fluorescence (Fig. 9).[42,43] Indeed, the similarities in emission behaviour of **D50% + ACM** in both THF and H_2O further confirm the attachment of the ACM moieties to the core block of the diblock copolymer nano-objects. In addition the blue shift in emission between the free dye in water and the dye inside the nanostructure cores implies the polarity of the latter resembles that of THF.

Fluorescence lifetime measurements displayed vast discrepancies depending on the solvent and/or attachment of the ACM dyes (Fig. S19A and Table S2†). Both **D20% + ACM** and **D50% + ACM** had similar average fluorescence lifetimes ($\tau_{Av,a}$) of 6.5 and 7.7 ns, respectively, and exhibited shorter lifetimes than the free dye in THF that had a $\tau_{Av,a}$ = 14.8 ns, providing further evidence of ACM's attachment to the diblock copolymers. To further investigate the influence of the spatial location of the dye, **D20%** or **D50%** were mixed with the appropriate quantity of free ACM in THF, displaying lifetimes of 13.8 and 14.2 ns, respectively, showing no differences between the free and polymer-bound dyes. This reinforced the idea that the observed decrease of lifetime in the initial study occurred as a consequence of the dye being in close proximity to the polymer chains (Fig. S19B†). Fluorescence lifetime measurements of **D20% + ACM**, **D50% + ACM** or free dye in water were very short – around 1 ns – indicating the dye was readily quenched regardless of attachment. Maleimide dyes are effectively quenched in protic solvents as a consequence of electron driven proton transfer from the hydrogen bonding between water and the fluorophore (Fig. S19C†).[45] Thus, the fact that reduced lifetimes were observed for **D20% + ACM** and **D50% + ACM** implied the presence of water in the nanoparticle cores was sufficient in quantity to quench fluorescence.

Conclusions

Helical-core micelles that could easily be functionalised by different nucleophiles were synthesised *via* copolymerisation

of **FAIC** and **MAIC** aryl isocyanide monomers by NiCCo-PISA. The resulting diblock copolymers and nanostructures were analysed by complementary techniques, showing the successful introduction of a range of functionalities by PPM including alcohols, fluorinated units and fluorescent dyes. Moreover, the stability of the core's helicity to the PPM conditions was confirmed. The PFP units inside the hydrophobic core were shown to be resistant to hydrolysis under the reaction conditions and during dialysis, indicating that these micelles could be employed for modification under aqueous conditions. When hydrophilic amines were utilised (*i.e.* EOA and ACM), partial disassembly of the micelles was observed for the **D50%** diblock copolymer nano-objects, demonstrating the effect of the modification of the core's polarity on the nano-objects' structural integrity. The introduction of ACM inside the micelle cores confirmed, *via* solvatochromatism, their covalent attachment within the hydrophobic cores of the nanostructures. Lifetime measurements indicated the presence of water in the core that readily quenched the grafted dyes. These micelles represent versatile helical scaffolds for the preparation of functionalised nanostructures, with potential applications as chiral fluorescent probes, enantiomer-specific stimuli-responsive systems or stereoselective nanoreactors.

Conflicts of interest

There are no conflicts to declare.

Acknowledgements

This work was supported by the European Union (SUSPOL-EJD 642671), ERC (grant number 615142), EPSRC and the University of Birmingham.

Notes and references

1 J.-F. Lutz and B. S. Sumerlin, The Role of Click Chemistry in Polymer Synthesis, in *Click Chemistry for Biotechnology and Materials Science*, ed. J. Lahann, John Wiley & Sons, Ltd., 2009, pp. 69–88.
2 N. K. Boaen and M. A. Hillmyer, *Chem. Soc. Rev.*, 2005, **34**, 267–275.
3 M. A. Gauthier, M. I. Gibson and H.-A. Klok, *Angew. Chem., Int. Ed.*, 2009, **48**, 48–58.
4 K. A. Günay, P. Theato and H.-A. Klok, *J. Polym. Sci., Part A: Polym. Chem.*, 2013, **51**, 1–28.
5 M. B. Larsen, S.-J. Wang and M. A. Hillmyer, *J. Am. Chem. Soc.*, 2018, **140**, 11911–11915.
6 C. J. Atkins, G. Patias, J. S. Town, A. M. Wemyss, A. M. Eissa, A. Shegiwal and D. M. Haddleton, *Polym. Chem.*, 2019, **10**, 646–655.
7 T. Krappitz, P. Feibusch, C. Aroonsirichock, V. P. Hoven and P. Theato, *Macromolecules*, 2017, **50**, 1415–1421.
8 P. K. Kuroishi, M. J. Bennison and A. P. Dove, *Polym. Chem.*, 2016, **7**, 7108–7115.
9 T. R. Barlow, J. C. Brendel and S. Perrier, *Macromolecules*, 2016, **49**, 6203–6212.
10 R. J. Ono, S. Q. Liu, S. Venkataraman, W. Chin, Y. Y. Yang and J. L. Hedrick, *Macromolecules*, 2014, **47**, 7725–7731.
11 Y.-C. M. Wu and T. M. Swager, *J. Am. Chem. Soc.*, 2019, **141**, 12498–12501.
12 N. H. Park, M. Fevre, Z. X. Voo, R. J. Ono, Y. Y. Yang and J. L. Hedrick, *ACS Macro Lett.*, 2016, **5**, 1247–1252.
13 D. N. Crisan, O. Creese, R. Ball, J. L. Brioso, B. Martyn, J. Montenegro and F. Fernandez-Trillo, *Polym. Chem.*, 2017, **8**, 4576–4584.
14 P. R. Sruthi and S. Anas, *J. Polym. Sci.*, 2020, **58**, 1039–1061.
15 T. Kubo, C. A. Figg, J. L. Swartz, W. L. A. Brooks and B. S. Sumerlin, *Macromolecules*, 2016, **49**, 2077–2084.
16 C. Battistella, Y. Yang, J. Chen and H.-A. Klok, *ACS Omega*, 2018, **3**, 9710–9721.
17 A. Das and P. Theato, *Macromolecules*, 2015, **48**, 8695–8707.
18 M. P. Robin and R. K. O'Reilly, *Chem. Sci.*, 2014, **5**, 2717–2723.
19 Y. Zhong, B. J. Zeberl, X. Wang and J. Luo, *Acta Biomater.*, 2018, **73**, 21–37.
20 N. Busatto, J. L. Keddie and P. J. Roth, *Polym. Chem.*, 2020, **11**, 704–711.
21 X. Liu, D. Hu, Z. Jiang, J. Zhuang, Y. Xu, X. Guo and S. Thayumanavan, *Macromolecules*, 2016, **49**, 6186–6192.
22 P. Theato, B. S. Sumerlin, R. K. O'Reilly and T. H. Epps III, *Chem. Soc. Rev.*, 2013, **42**, 7055–7056.
23 M. S. Rolph, M. Inam and R. K. O'Reilly, *Polym. Chem.*, 2017, **8**, 7229–7239.
24 O. Rifaie-Graham, S. Ulrich, N. F. B. Galensowske, S. Balog, M. Chami, D. Rentsch, J. R. Hemmer, J. Read de Alaniz, L. F. Boesel and N. Bruns, *J. Am. Chem. Soc.*, 2018, **140**, 8027–8036.
25 S. Zhang, J. Zou, F. Zhang, M. Elsabahy, S. E. Felder, J. Zhu, D. J. Pochan and K. L. Wooley, *J. Am. Chem. Soc.*, 2012, **134**, 18467–18474.
26 Y. H. Lim, G. S. Heo, Y. H. Rezenom, S. Pollack, J. E. Raymond, M. Elsabahy and K. L. Wooley, *Macromolecules*, 2014, **47**, 4634–4644.
27 S. Cho, G. S. Heo, S. Khan, J. Huang, D. A. Hunstad, M. Elsabahy and K. L. Wooley, *Macromolecules*, 2018, **51**, 3233–3242.
28 F. D. Jochum and P. Theato, *Macromolecules*, 2009, **42**, 5941–5945.
29 Q. Zhang, P. Schattling, P. Theato and R. Hoogenboom, *Eur. Polym. J.*, 2015, **62**, 435–441.
30 H. Gaballa, S. Lin, J. Shang, S. Meier and P. Theato, *Polym. Chem.*, 2018, **9**, 3355–3358.
31 M. I. Gibson, E. Fröhlich and H.-A. Klok, *J. Polym. Sci., Part A: Polym. Chem.*, 2009, **47**, 4332–4345.
32 S. Lin, A. Das and P. Theato, *Polym. Chem.*, 2017, **8**, 1206–1216.

33 Y. Liu, T. Pauloehrl, S. I. Presolski, L. Albertazzi, A. R. A. Palmans and E. W. Meijer, *J. Am. Chem. Soc.*, 2015, **137**, 13096–13105.
34 B. Couturaud, P. G. Georgiou, S. Varlas, J. R. Jones, M. C. Arno, J. C. Foster and R. K. O'Reilly, *Macromol. Rapid Commun.*, 2019, **40**, 1800460.
35 S. Jimaja, S. Varlas, Y. Xie, J. C. Foster, D. Taton, A. P. Dove and R. K. O'Reilly, *ACS Macro Lett.*, 2020, **9**, 226–232.
36 N. Liu, C.-H. Ma, R.-W. Sun, J. Huang, C. Li and Z.-Q. Wu, *Polym. Chem.*, 2017, **8**, 2152–2163.
37 J. Yin, L. Xu, X. Han, L. Zhou, C. Li and Z.-Q. Wu, *Polym. Chem.*, 2017, **8**, 545–556.
38 L. Xu, X.-H. Xu, N. Liu, H. Zou and Z.-Q. Wu, *Macromolecules*, 2018, **51**, 7546–7555.
39 M. Su, N. Liu, Q. Wang, H. Wang, J. Yin and Z.-Q. Wu, *Macromolecules*, 2016, **49**, 110–119.
40 M. P. Robin, M. W. Jones, D. M. Haddleton and R. K. O'Reilly, *ACS Macro Lett.*, 2012, **1**, 222–226.
41 M. P. Robin, P. Wilson, A. B. Mabire, J. K. Kiviaho, J. E. Raymond, D. M. Haddleton and R. K. O'Reilly, *J. Am. Chem. Soc.*, 2013, **135**, 2875–2878.
42 A. B. Mabire, M. P. Robin, W.-D. Quan, H. Willcock, V. G. Stavros and R. K. O'Reilly, *Chem. Commun.*, 2015, **51**, 9733–9736.
43 Y. Xie, J. T. Husband, M. Torrent-Sucarrat, H. Yang, W. Liu and R. K. O'Reilly, *Chem. Commun.*, 2018, **54**, 3339–3342.
44 J. T. Husband, A. C. Hill and R. K. O'Reilly, *Polym. Int.*, 2019, **68**, 1247–1254.
45 M. Staniforth, W.-D. Quan, T. N. V. Karsili, L. A. Baker, R. K. O'Reilly and V. G. Stavros, *J. Phys. Chem. A*, 2017, **121**, 6357–6365.
46 S. Asaoka, A. Joza, S. Minagawa, L. Song, Y. Suzuki and T. Iyoda, *ACS Macro Lett.*, 2013, **2**, 906–911.
47 F. Takei, K. Yanai, K. Onitsuka and S. Takahashi, *Chem. – Eur. J.*, 2000, **6**, 983–993.
48 J. Lee, S. Shin and T.-L. Choi, *Macromolecules*, 2018, **51**, 7800–7806.